

# Measurement of $\phi_3$ with Dalitz Plot Analysis of $B^\pm \rightarrow D^{(*)}K^\pm$ Decay at Belle

K. Abe,<sup>10</sup> K. Abe,<sup>46</sup> N. Abe,<sup>49</sup> I. Adachi,<sup>10</sup> H. Aihara,<sup>48</sup> M. Akatsu,<sup>24</sup> Y. Asano,<sup>53</sup>  
T. Aso,<sup>52</sup> V. Aulchenko,<sup>2</sup> T. Aushev,<sup>14</sup> T. Aziz,<sup>44</sup> S. Bahinipati,<sup>6</sup> A. M. Bakich,<sup>43</sup>  
Y. Ban,<sup>36</sup> M. Barbero,<sup>9</sup> A. Bay,<sup>20</sup> I. Bedny,<sup>2</sup> U. Bitenc,<sup>15</sup> I. Bizjak,<sup>15</sup> S. Blyth,<sup>29</sup>  
A. Bondar,<sup>2</sup> A. Bozek,<sup>30</sup> M. Bračko,<sup>22,15</sup> J. Brodzicka,<sup>30</sup> T. E. Browder,<sup>9</sup> M.-C. Chang,<sup>29</sup>  
P. Chang,<sup>29</sup> Y. Chao,<sup>29</sup> A. Chen,<sup>26</sup> K.-F. Chen,<sup>29</sup> W. T. Chen,<sup>26</sup> B. G. Cheon,<sup>4</sup>  
R. Chistov,<sup>14</sup> S.-K. Choi,<sup>8</sup> Y. Choi,<sup>42</sup> Y. K. Choi,<sup>42</sup> A. Chuvikov,<sup>37</sup> S. Cole,<sup>43</sup>  
M. Danilov,<sup>14</sup> M. Dash,<sup>55</sup> L. Y. Dong,<sup>12</sup> R. Dowd,<sup>23</sup> J. Dragic,<sup>23</sup> A. Drutskoy,<sup>6</sup>  
S. Eidelman,<sup>2</sup> Y. Enari,<sup>24</sup> D. Epifanov,<sup>2</sup> C. W. Everton,<sup>23</sup> F. Fang,<sup>9</sup> S. Fratina,<sup>15</sup>  
H. Fujii,<sup>10</sup> N. Gabyshev,<sup>2</sup> A. Garmash,<sup>37</sup> T. Gershon,<sup>10</sup> A. Go,<sup>26</sup> G. Gokhroo,<sup>44</sup>  
B. Golob,<sup>21,15</sup> M. Grosse Perdekamp,<sup>38</sup> H. Guler,<sup>9</sup> J. Haba,<sup>10</sup> F. Handa,<sup>47</sup> K. Hara,<sup>10</sup>  
T. Hara,<sup>34</sup> N. C. Hastings,<sup>10</sup> K. Hasuko,<sup>38</sup> K. Hayasaka,<sup>24</sup> H. Hayashii,<sup>25</sup> M. Hazumi,<sup>10</sup>  
E. M. Heenan,<sup>23</sup> I. Higuchi,<sup>47</sup> T. Higuchi,<sup>10</sup> L. Hinz,<sup>20</sup> T. Hojo,<sup>34</sup> T. Hokuue,<sup>24</sup>  
Y. Hoshi,<sup>46</sup> K. Hoshina,<sup>51</sup> S. Hou,<sup>26</sup> W.-S. Hou,<sup>29</sup> Y. B. Hsiung,<sup>29</sup> H.-C. Huang,<sup>29</sup>  
T. Igaki,<sup>24</sup> Y. Igarashi,<sup>10</sup> T. Iijima,<sup>24</sup> A. Imoto,<sup>25</sup> K. Inami,<sup>24</sup> A. Ishikawa,<sup>10</sup> H. Ishino,<sup>49</sup>  
K. Itoh,<sup>48</sup> R. Itoh,<sup>10</sup> M. Iwamoto,<sup>3</sup> M. Iwasaki,<sup>48</sup> Y. Iwasaki,<sup>10</sup> R. Kagan,<sup>14</sup> H. Kakuno,<sup>48</sup>  
J. H. Kang,<sup>56</sup> J. S. Kang,<sup>17</sup> P. Kapusta,<sup>30</sup> S. U. Kataoka,<sup>25</sup> N. Katayama,<sup>10</sup> H. Kawai,<sup>3</sup>  
H. Kawai,<sup>48</sup> Y. Kawakami,<sup>24</sup> N. Kawamura,<sup>1</sup> T. Kawasaki,<sup>32</sup> N. Kent,<sup>9</sup> H. R. Khan,<sup>49</sup>  
A. Kibayashi,<sup>49</sup> H. Kichimi,<sup>10</sup> H. J. Kim,<sup>19</sup> H. O. Kim,<sup>42</sup> Hyunwoo Kim,<sup>17</sup> J. H. Kim,<sup>42</sup>  
S. K. Kim,<sup>41</sup> T. H. Kim,<sup>56</sup> K. Kinoshita,<sup>6</sup> P. Koppenburg,<sup>10</sup> S. Korpar,<sup>22,15</sup> P. Križan,<sup>21,15</sup>  
P. Krokovny,<sup>2</sup> R. Kulasiri,<sup>6</sup> C. C. Kuo,<sup>26</sup> H. Kurashiro,<sup>49</sup> E. Kurihara,<sup>3</sup> A. Kusaka,<sup>48</sup>  
A. Kuzmin,<sup>2</sup> Y.-J. Kwon,<sup>56</sup> J. S. Lange,<sup>7</sup> G. Leder,<sup>13</sup> S. E. Lee,<sup>41</sup> S. H. Lee,<sup>41</sup>  
Y.-J. Lee,<sup>29</sup> T. Lesiak,<sup>30</sup> J. Li,<sup>40</sup> A. Limosani,<sup>23</sup> S.-W. Lin,<sup>29</sup> D. Liventsev,<sup>14</sup>  
J. MacNaughton,<sup>13</sup> G. Majumder,<sup>44</sup> F. Mandl,<sup>13</sup> D. Marlow,<sup>37</sup> T. Matsuishi,<sup>24</sup>  
H. Matsumoto,<sup>32</sup> S. Matsumoto,<sup>5</sup> T. Matsumoto,<sup>50</sup> A. Matyja,<sup>30</sup> Y. Mikami,<sup>47</sup>  
W. Mitaroff,<sup>13</sup> K. Miyabayashi,<sup>25</sup> Y. Miyabayashi,<sup>24</sup> H. Miyake,<sup>34</sup> H. Miyata,<sup>32</sup> R. Mizuk,<sup>14</sup>  
D. Mohapatra,<sup>55</sup> G. R. Moloney,<sup>23</sup> G. F. Moorhead,<sup>23</sup> T. Mori,<sup>49</sup> A. Murakami,<sup>39</sup>  
T. Nagamine,<sup>47</sup> Y. Nagasaka,<sup>11</sup> T. Nakadaira,<sup>48</sup> I. Nakamura,<sup>10</sup> E. Nakano,<sup>33</sup> M. Nakao,<sup>10</sup>  
H. Nakazawa,<sup>10</sup> Z. Natkaniec,<sup>30</sup> K. Neichi,<sup>46</sup> S. Nishida,<sup>10</sup> O. Nitoh,<sup>51</sup> S. Noguchi,<sup>25</sup>  
T. Nozaki,<sup>10</sup> A. Ogawa,<sup>38</sup> S. Ogawa,<sup>45</sup> T. Ohshima,<sup>24</sup> T. Okabe,<sup>24</sup> S. Okuno,<sup>16</sup>  
S. L. Olsen,<sup>9</sup> Y. Onuki,<sup>32</sup> W. Ostrowicz,<sup>30</sup> H. Ozaki,<sup>10</sup> P. Pakhlov,<sup>14</sup> H. Palka,<sup>30</sup>  
C. W. Park,<sup>42</sup> H. Park,<sup>19</sup> K. S. Park,<sup>42</sup> N. Parslow,<sup>43</sup> L. S. Peak,<sup>43</sup> M. Pernicka,<sup>13</sup>  
J.-P. Perroud,<sup>20</sup> M. Peters,<sup>9</sup> L. E. Piilonen,<sup>55</sup> A. Poluektov,<sup>2</sup> F. J. Ronga,<sup>10</sup> N. Root,<sup>2</sup>  
M. Rozanska,<sup>30</sup> H. Sagawa,<sup>10</sup> M. Saigo,<sup>47</sup> S. Saitoh,<sup>10</sup> Y. Sakai,<sup>10</sup> H. Sakamoto,<sup>18</sup>  
T. R. Sarangi,<sup>10</sup> M. Satopathy,<sup>54</sup> N. Sato,<sup>24</sup> O. Schneider,<sup>20</sup> J. Schümann,<sup>29</sup> C. Schwanda,<sup>13</sup>  
A. J. Schwartz,<sup>6</sup> T. Seki,<sup>50</sup> S. Semenov,<sup>14</sup> K. Senyo,<sup>24</sup> Y. Settai,<sup>5</sup> R. Seuster,<sup>9</sup>  
M. E. Sevier,<sup>23</sup> T. Shibata,<sup>32</sup> H. Shibuya,<sup>45</sup> B. Shwartz,<sup>2</sup> V. Sidorov,<sup>2</sup> V. Siegle,<sup>38</sup>  
J. B. Singh,<sup>35</sup> A. Somov,<sup>6</sup> N. Soni,<sup>35</sup> R. Stamen,<sup>10</sup> S. Stanič,<sup>53,\*</sup> M. Starič,<sup>15</sup> A. Sugi,<sup>24</sup>  
A. Sugiyama,<sup>39</sup> K. Sumisawa,<sup>34</sup> T. Sumiyoshi,<sup>50</sup> S. Suzuki,<sup>39</sup> S. Y. Suzuki,<sup>10</sup> O. Tajima,<sup>10</sup>  
F. Takasaki,<sup>10</sup> K. Tamai,<sup>10</sup> N. Tamura,<sup>32</sup> K. Tanabe,<sup>48</sup> M. Tanaka,<sup>10</sup> G. N. Taylor,<sup>23</sup>  
Y. Teramoto,<sup>33</sup> X. C. Tian,<sup>36</sup> S. Tokuda,<sup>24</sup> S. N. Tovey,<sup>23</sup> K. Trabelsi,<sup>9</sup> T. Tsuboyama,<sup>10</sup>  
T. Tsukamoto,<sup>10</sup> K. Uchida,<sup>9</sup> S. Uehara,<sup>10</sup> T. Uglov,<sup>14</sup> K. Ueno,<sup>29</sup> Y. Unno,<sup>3</sup> S. Uno,<sup>10</sup>

Y. Ushiroda,<sup>10</sup> G. Varner,<sup>9</sup> K. E. Varvell,<sup>43</sup> S. Villa,<sup>20</sup> C. C. Wang,<sup>29</sup> C. H. Wang,<sup>28</sup>  
J. G. Wang,<sup>55</sup> M.-Z. Wang,<sup>29</sup> M. Watanabe,<sup>32</sup> Y. Watanabe,<sup>49</sup> L. Widhalm,<sup>13</sup>  
Q. L. Xie,<sup>12</sup> B. D. Yabsley,<sup>55</sup> A. Yamaguchi,<sup>47</sup> H. Yamamoto,<sup>47</sup> S. Yamamoto,<sup>50</sup>  
T. Yamanaka,<sup>34</sup> Y. Yamashita,<sup>31</sup> M. Yamauchi,<sup>10</sup> Heyoung Yang,<sup>41</sup> P. Yeh,<sup>29</sup> J. Ying,<sup>36</sup>  
K. Yoshida,<sup>24</sup> Y. Yuan,<sup>12</sup> Y. Yusa,<sup>47</sup> H. Yuta,<sup>1</sup> S. L. Zang,<sup>12</sup> C. C. Zhang,<sup>12</sup> J. Zhang,<sup>10</sup>  
L. M. Zhang,<sup>40</sup> Z. P. Zhang,<sup>40</sup> V. Zhilich,<sup>2</sup> T. Ziegler,<sup>37</sup> D. Žontar,<sup>21,15</sup> and D. Zürcher<sup>20</sup>

(The Belle Collaboration)

<sup>1</sup>*Aomori University, Aomori*

<sup>2</sup>*Budker Institute of Nuclear Physics, Novosibirsk*

<sup>3</sup>*Chiba University, Chiba*

<sup>4</sup>*Chonnam National University, Kwangju*

<sup>5</sup>*Chuo University, Tokyo*

<sup>6</sup>*University of Cincinnati, Cincinnati, Ohio 45221*

<sup>7</sup>*University of Frankfurt, Frankfurt*

<sup>8</sup>*Gyeongsang National University, Chinju*

<sup>9</sup>*University of Hawaii, Honolulu, Hawaii 96822*

<sup>10</sup>*High Energy Accelerator Research Organization (KEK), Tsukuba*

<sup>11</sup>*Hiroshima Institute of Technology, Hiroshima*

<sup>12</sup>*Institute of High Energy Physics,*

*Chinese Academy of Sciences, Beijing*

<sup>13</sup>*Institute of High Energy Physics, Vienna*

<sup>14</sup>*Institute for Theoretical and Experimental Physics, Moscow*

<sup>15</sup>*J. Stefan Institute, Ljubljana*

<sup>16</sup>*Kanagawa University, Yokohama*

<sup>17</sup>*Korea University, Seoul*

<sup>18</sup>*Kyoto University, Kyoto*

<sup>19</sup>*Kyungpook National University, Taegu*

<sup>20</sup>*Swiss Federal Institute of Technology of Lausanne, EPFL, Lausanne*

<sup>21</sup>*University of Ljubljana, Ljubljana*

<sup>22</sup>*University of Maribor, Maribor*

<sup>23</sup>*University of Melbourne, Victoria*

<sup>24</sup>*Nagoya University, Nagoya*

<sup>25</sup>*Nara Women's University, Nara*

<sup>26</sup>*National Central University, Chung-li*

<sup>27</sup>*National Kaohsiung Normal University, Kaohsiung*

<sup>28</sup>*National United University, Miao Li*

<sup>29</sup>*Department of Physics, National Taiwan University, Taipei*

<sup>30</sup>*H. Niewodniczanski Institute of Nuclear Physics, Krakow*

<sup>31</sup>*Nihon Dental College, Niigata*

<sup>32</sup>*Niigata University, Niigata*

<sup>33</sup>*Osaka City University, Osaka*

<sup>34</sup>*Osaka University, Osaka*

<sup>35</sup>*Panjab University, Chandigarh*

<sup>36</sup>*Peking University, Beijing*

<sup>37</sup>*Princeton University, Princeton, New Jersey 08545*

<sup>38</sup>*RIKEN BNL Research Center, Upton, New York 11973*

- <sup>39</sup>*Saga University, Saga*  
<sup>40</sup>*University of Science and Technology of China, Hefei*  
<sup>41</sup>*Seoul National University, Seoul*  
<sup>42</sup>*Sungkyunkwan University, Suwon*  
<sup>43</sup>*University of Sydney, Sydney NSW*  
<sup>44</sup>*Tata Institute of Fundamental Research, Bombay*  
<sup>45</sup>*Toho University, Funabashi*  
<sup>46</sup>*Tohoku Gakuin University, Tagajo*  
<sup>47</sup>*Tohoku University, Sendai*  
<sup>48</sup>*Department of Physics, University of Tokyo, Tokyo*  
<sup>49</sup>*Tokyo Institute of Technology, Tokyo*  
<sup>50</sup>*Tokyo Metropolitan University, Tokyo*  
<sup>51</sup>*Tokyo University of Agriculture and Technology, Tokyo*  
<sup>52</sup>*Toyama National College of Maritime Technology, Toyama*  
<sup>53</sup>*University of Tsukuba, Tsukuba*  
<sup>54</sup>*Utkal University, Bhubaneswer*  
<sup>55</sup>*Virginia Polytechnic Institute and State University, Blacksburg, Virginia 24061*  
<sup>56</sup>*Yonsei University, Seoul*
- (Dated: October 25, 2018)

## Abstract

We present a measurement of the unitarity triangle angle  $\phi_3$  using a Dalitz plot analysis of the three-body decay of the neutral  $D$  meson from the  $B^\pm \rightarrow D^{(*)}K^\pm$  process. Using a  $253 \text{ fb}^{-1}$  data sample collected by the Belle experiment, we obtain 276 signal candidates for  $B^\pm \rightarrow DK^\pm$  and 69 candidates for  $B^\pm \rightarrow D^*K^\pm$ , where the neutral  $D$  meson decays into  $K_S\pi^+\pi^-$ . From a combined maximum likelihood fit to the  $B^\pm \rightarrow DK^\pm$  and  $B^\pm \rightarrow D^*K^\pm$  modes, we obtain  $\phi_3 = 68^\circ \text{ }^{+14^\circ}_{-15^\circ}(\text{stat}) \pm 13^\circ(\text{syst}) \pm 11^\circ(\text{model})$ . The corresponding two standard deviation interval is  $22^\circ < \phi_3 < 113^\circ$ .

## INTRODUCTION

Determinations of the Cabbibo-Kobayashi-Maskawa (CKM) [1] matrix elements provide important checks on the consistency of the Standard Model and ways to search for new physics. Various methods using  $CP$  violation in  $B \rightarrow DK$  decays have been proposed [2, 3, 4, 5] to measure the unitarity triangle angle  $\phi_3$ . These methods are based on two key observations: neutral  $D^0$  and  $\bar{D}^0$  mesons can decay to a common final state, and the decay  $B^+ \rightarrow D^{(*)}K^+$  can produce neutral  $D$  mesons of both flavors via  $\bar{b} \rightarrow \bar{c}u\bar{s}$  (Fig. 1a) and  $\bar{b} \rightarrow \bar{u}c\bar{s}$  (Fig. 1b) transitions, with a relative phase  $\theta_+$  between the two interfering amplitudes that is the sum,  $\delta + \phi_3$ , of strong and weak interaction phases. For the charge conjugate mode, the relative phase is  $\theta_- = \delta - \phi_3$ .

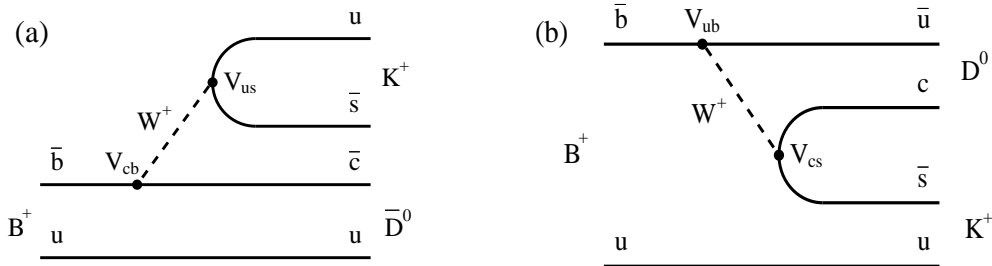


FIG. 1: Feynman diagrams of (a) dominant  $B^+ \rightarrow \bar{D}^0 K^+$  and (b) suppressed  $B^+ \rightarrow D^0 K^+$  decays

Recently, three body final states common to  $D^0$  and  $\bar{D}^0$ , such as  $K_S \pi^+ \pi^-$  [6], were suggested as promising modes for the extraction of  $\phi_3$ . In the Wolfenstein parameterization of the CKM matrix elements, the amplitudes of the two diagrams that contribute to the decay  $B^+ \rightarrow DK^+$  are given by  $M_1 \sim V_{cb}^* V_{us} \sim A\lambda^3$  (for the  $\bar{D}^0 K^+$  final state) and  $M_2 \sim V_{ub}^* V_{cs} \sim A\lambda^3(\rho + i\eta)$  (for  $D^0 K^+$ ). The two amplitudes  $M_1$  and  $M_2$  interfere as the  $D^0$  and  $\bar{D}^0$  mesons decay into the same final state  $K_S \pi^+ \pi^-$ ; we denote the admixed state as  $\tilde{D}$ . Assuming no  $CP$  asymmetry in neutral  $D$  decays, the amplitude of the  $B^+$  decay can be written as

$$M_+ = f(m_+^2, m_-^2) + r e^{i\phi_3 + i\delta} f(m_-^2, m_+^2) \quad (1)$$

and the corresponding amplitude for the charge conjugate  $B^-$  decay is can be written as

$$M_- = f(m_-^2, m_+^2) + r e^{-i\phi_3 + i\delta} f(m_+^2, m_-^2), \quad (2)$$

where  $m_+^2$  and  $m_-^2$  are the squared invariant masses of the  $K_S \pi^+$  and  $K_S \pi^-$  combinations, respectively, and  $f(m_+, m_-)$  is the complex amplitude for the  $\bar{D}^0 \rightarrow K_S \pi^+ \pi^-$  decay. The absolute value of the ratio between the two interfering amplitudes,  $r$ , is predicted to be 0.1–0.2.

Once the functional form of  $f$  is fixed by a  $\bar{D}^0 \rightarrow K_S \pi^+ \pi^-$  decay model, the  $\tilde{D}$  Dalitz distributions for the  $B^+$  and  $B^-$  decays can be fitted simultaneously using the above expressions with  $r$ ,  $\phi_3$ , and  $\delta$  as free parameters. The  $\bar{D}^0 \rightarrow K_S \pi^+ \pi^-$  decay model can be determined from a large sample of flavor-tagged  $\bar{D}^0 \rightarrow K_S \pi^+ \pi^-$  decays produced in continuum  $e^+ e^-$  annihilation.

The current measurement is an update of our analysis [7], which was based on 140  $\text{fb}^{-1}$  data sample. Both measurements are based on two decay modes,  $B^\pm \rightarrow \tilde{D} K^\pm$  and  $B^\pm \rightarrow \tilde{D}^* K^\pm$  ( $D^* \rightarrow D\pi^0$ ). Recently, the same technique has been applied by the BABAR collaboration [8] with consistent results.

## EVENT SELECTION

We use a  $253 \text{ fb}^{-1}$  data sample, corresponding to  $275 \times 10^6 B\bar{B}$  pairs, collected by the Belle detector. The decays  $B^\pm \rightarrow DK^\pm$  and  $B^\pm \rightarrow D^*K^\pm$ ,  $D^* \rightarrow D\pi^0$  are selected for the determination of  $\phi_3$ ; the decays  $B^\pm \rightarrow D\pi^\pm$  and  $B^\pm \rightarrow D^*\pi^\pm$  with  $D^* \rightarrow D\pi^0$  serve as control samples. We require the neutral  $D$  meson to decay to the  $K_S\pi^+\pi^-$  final state in all cases. We also select decays of  $D^{*\pm} \rightarrow D\pi^\pm$  produced via the  $e^+e^- \rightarrow c\bar{c}$  continuum process as a high-statistics sample to determine the  $\bar{D}^0 \rightarrow K_S\pi^+\pi^-$  decay amplitude. The Belle detector is described in detail elsewhere [9]. The event selection procedures are the same as was described in the previous analysis [7].

We use  $\Delta M = M_{K_S\pi^+\pi^-\pi_s^\pm} - M_{K_S\pi^+\pi^-}$  and  $M_{K_S\pi^+\pi^-}$  distributions to select the  $D^{*\pm} \rightarrow D\pi_s^\pm$  events, where  $\pi_s^\pm$  stands for ‘‘slow pion’’ that is a distinct signature for this decay. The fit to the  $\Delta M$  distribution yields  $186854 \pm 856$  signal events and  $6126 \pm 65$  background events in the signal region ( $144.6 \text{ MeV}/c^2 < \Delta M < 146.4 \text{ MeV}/c^2$ ). The corresponding background fraction is 3.2%.

The selection of  $B$  candidates is based on the CM energy difference  $\Delta E = \sum E_i - E_{\text{beam}}$  and the beam-constrained  $B$  meson mass  $M_{\text{bc}} = \sqrt{E_{\text{beam}}^2 - (\sum p_i)^2}$ , where  $E_{\text{beam}}$  is the CM beam energy, and  $E_i$  and  $p_i$  are the CM energies and momenta of the  $B$  candidate decay products. The requirements for signal candidates are  $5.272 \text{ GeV}/c^2 < M_{\text{bc}} < 5.288 \text{ GeV}/c^2$  and  $|\Delta E| < 0.022 \text{ GeV}$ . The  $\Delta E$  and  $M_{\text{bc}}$  distributions for  $B^\pm \rightarrow DK^\pm$  candidates are shown in Fig. 2. The peak in the  $\Delta E$  distribution at  $\Delta E = 50 \text{ MeV}$  is due to  $B^\pm \rightarrow D\pi^\pm$  decays, where the pion is misidentified as a kaon. The  $B^\pm \rightarrow DK^\pm$  selection efficiency (11%) is determined from a Monte Carlo (MC) simulation. The number of events passing all selection criteria is 276. The background fraction is determined from a binned fit to the  $\Delta E$  distribution, in which the signal is represented by a Gaussian distribution with mean  $\Delta E = 0$ , the  $B^\pm \rightarrow D\pi^\pm$  component is represented by a Gaussian distribution with mean  $\Delta E = 50 \text{ MeV}$  and the remaining background is modeled by a linear function. The contributions in the signal region are found to be  $209 \pm 16$  signal events,  $2.6 \pm 0.3 B^\pm \rightarrow D\pi^\pm$  events and  $65 \pm 5$  events in the linear background. The overall background fraction is  $25 \pm 2\%$ .

Figure 3 shows the  $\Delta E$ ,  $M_{\text{bc}}$  and  $\Delta M$  distributions for  $B^\pm \rightarrow D^*K^\pm$  candidates. The selection efficiency is 6.2%. The number of events satisfying the selection criteria is 69. The background fraction is determined in the same way as for  $B^\pm \rightarrow DK^\pm$  events. The fit of the  $\Delta E$  distribution yields  $58 \pm 8$  signal events,  $8.3 \pm 1.5$  events corresponding to the linear background and  $0.44 \pm 0.10 B^\pm \rightarrow D^*\pi^\pm$  events in the signal region. The background fraction is  $13 \pm 2\%$ .

## DETERMINATION OF $\bar{D}^0 \rightarrow K_S\pi^+\pi^-$ DECAY MODEL

The amplitude  $f$  of the  $\bar{D}^0 \rightarrow K_S\pi^+\pi^-$  decay is represented by a coherent sum of two-body decay amplitudes plus one non-resonant decay amplitude,

$$f(m_+^2, m_-^2) = \sum_{j=1}^N a_j e^{i\alpha_j} \mathcal{A}_j(m_+^2, m_-^2) + b e^{i\beta}, \quad (3)$$

where  $N$  is the total number of resonances,  $\mathcal{A}_j(m_+^2, m_-^2)$ ,  $a_j$  and  $\alpha_j$  are the matrix element, amplitude and phase, respectively, of the  $j$ -th resonance, and  $b$  and  $\beta$  are the amplitude and phase of the non-resonant component. The total phase and amplitude are arbitrary. To

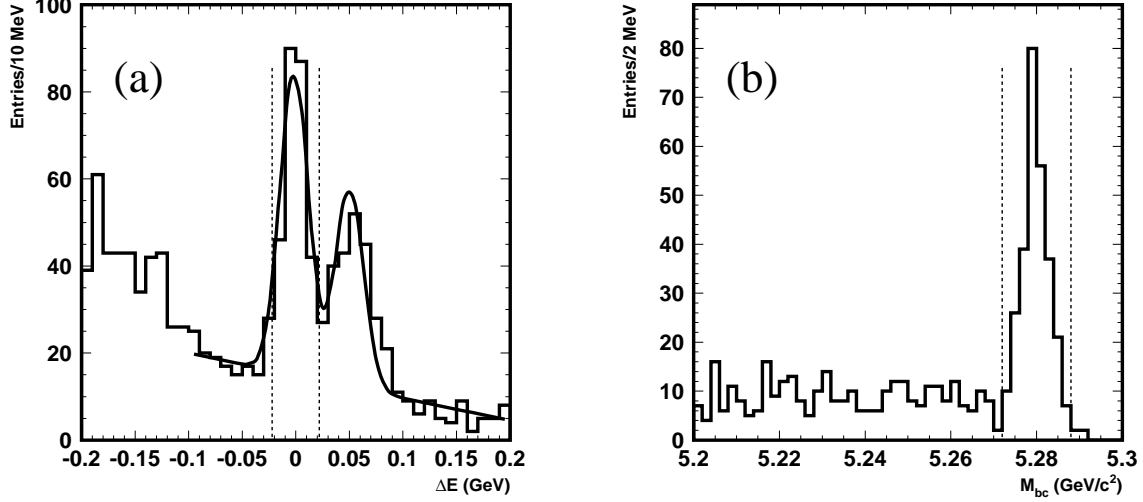


FIG. 2: (a)  $\Delta E$  and (b)  $M_{bc}$  distributions for the  $B^\pm \rightarrow DK^\pm$  candidates. Dashed lines show the signal region. The histogram shows the data; the smooth curve in (a) is the fit result.

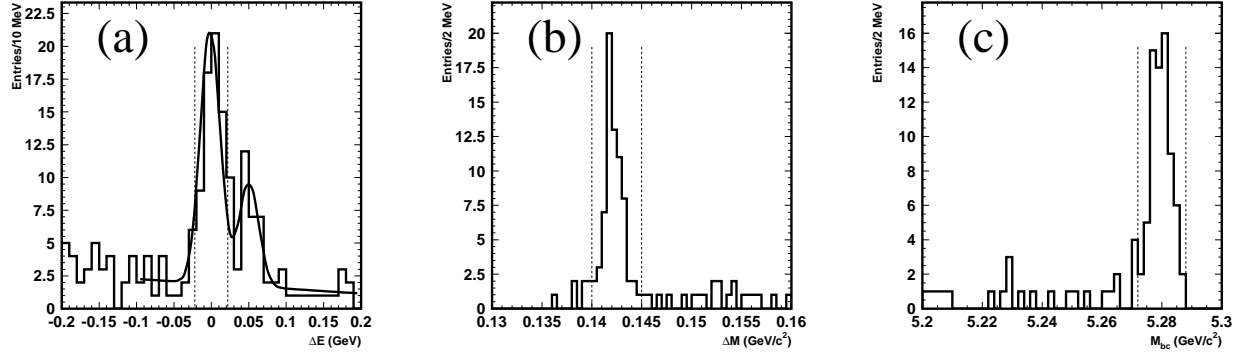


FIG. 3: (a)  $\Delta E$ , (b)  $\Delta M$  and (c)  $M_{bc}$  distributions for the  $B^\pm \rightarrow D^*K^\pm$  candidates. Dashed lines show the signal region. The histogram shows the data; the smooth curve in (a) is the fit result.

be consistent with other analyses [8, 10] we have chosen the  $\bar{D}^0 \rightarrow K_S \rho$  mode to have unit amplitude and zero relative phase. The description of the matrix elements follows Ref. [11].

For the  $\bar{D}^0$  model we use a set of 18 two-body amplitudes. These include five Cabibbo-allowed amplitudes:  $K^*(892)^+\pi^-$ ,  $K^*(1410)^+\pi^-$ ,  $K_0^*(1430)^+\pi^-$ ,  $K_2^*(1430)^+\pi^-$  and  $K^*(1680)^+\pi^-$ ; their doubly Cabibbo-suppressed partners; and eight amplitudes with  $K_S$  and a  $\pi\pi$  resonance:  $K_S\rho$ ,  $K_S\omega$ ,  $K_S f_0(980)$ ,  $K_S f_2(1270)$ ,  $K_S f_0(1370)$ ,  $K_S\rho(1450)$ ,  $K_S\sigma_1$  and  $K_S\sigma_2$ . The differences from our previous analysis [7] are, i) addition of  $K_S\rho(1450)$ ,  $K^*(1410)^+\pi^-$  and its doubly Cabibbo-suppressed mode, ii) use of the Gounaris-Sakurai [12] amplitude description for the  $K_S\rho$  and  $K_S\rho(1450)$  contributions, and iii) the mass and width for the  $f_0(1370)$  state taken from [13] ( $M = 1434 \text{ MeV}/c^2$ ,  $\Gamma = 173 \text{ MeV}/c^2$ ).

We use an unbinned maximum likelihood technique to fit the Dalitz plot distribution to the model described by Eq. 3. We minimize the inverse logarithm of the likelihood function



in the form

$$-2 \log L = -2 \left[ \sum_{i=1}^n \log p(m_{+,i}^2, m_{-,i}^2) - \log \int_D p(m_+^2, m_-^2) dm_+^2 dm_-^2 \right], \quad (4)$$

where  $i$  runs over all selected event candidates, and  $m_{+,i}^2, m_{-,i}^2$  are measured Dalitz plot variables. The integral in the second term accounts for the overall normalization of the probability density.

The Dalitz plot density is represented by

$$p(m_+^2, m_-^2) = \varepsilon(m_+^2, m_-^2) \int_{-\infty}^{\infty} |M(m_+^2 + \mu^2, m_-^2 + \mu^2)|^2 \exp\left(-\frac{\mu^2}{2\sigma_m^2(m_{\pi\pi}^2)}\right) d\mu^2 + B(m_+^2, m_-^2), \quad (5)$$

where  $M(m_+^2, m_-^2) = f(m_+^2, m_-^2)$  is the decay amplitude described by Eq. 3,  $\varepsilon(m_+^2, m_-^2)$  is the efficiency,  $B(m_+^2, m_-^2)$  is the background density,  $\sigma_m(m_{\pi\pi}^2)$  is the resolution of the squared invariant mass  $m_{\pi\pi}^2$  of two pions ( $m_{\pi\pi}^2 = M_D^2 + M_K^2 + 2M_\pi^2 - m_+^2 - m_-^2$ ). The free parameters of the minimization are the amplitudes  $a_j$  and phases  $\alpha_j$  of the resonances (except for the  $K_S\rho$  component, for which the parameters are fixed), the amplitude  $b$  and phase  $\beta$  of the non-resonant component and the masses and widths of the  $\sigma_1$  and  $\sigma_2$  scalars.

The procedures for determining the background density, the efficiency, and the resolution of the squared invariant mass, are the same as in the previous analysis. The  $\bar{D}^0 \rightarrow K_S\pi^+\pi^-$  Dalitz plot distribution, as well as its projections with the fit results superimposed, are shown in Fig. 4. The fit results are given in Table I. The parameters of the  $\sigma$  resonances obtained in the fit are:  $M_{\sigma_1} = 520 \pm 15$  MeV/ $c^2$ ,  $\Gamma_{\sigma_1} = 466 \pm 31$  MeV/ $c^2$ ,  $M_{\sigma_2} = 1059 \pm 6$  MeV/ $c^2$ , and  $\Gamma_{\sigma_2} = 59 \pm 10$  MeV/ $c^2$ . The large peak in the  $m_+^2$  distribution corresponds to the dominant  $\bar{D}^0 \rightarrow K^*(892)^+\pi^-$  mode. The minimum in the  $m_-^2$  distribution at 0.8 GeV $^2/c^4$  is due to destructive interference with the doubly Cabibbo suppressed  $\bar{D}^0 \rightarrow K^*(892)^-\pi^+$  amplitude. In the  $m_{\pi\pi}^2$  distribution, the  $\bar{D}^0 \rightarrow K_S\rho$  contribution is visible around 0.5 GeV $^2/c^4$  with a steep edge on the upper side due to interference with  $\bar{D}^0 \rightarrow K_S\omega$ . The minimum around 0.9 GeV $^2/c^4$  is due to the decay  $\bar{D}^0 \rightarrow K_S f_0(980)$  interfering destructively with other modes.

The unbinned likelihood technique does not provide a reliable criterion for the goodness of fit. To check the quality of the fit, we make use of the large number of events in our sample and perform a binned  $\chi^2$  test by dividing the Dalitz plot into square regions  $0.05 \times 0.05$  GeV $^2/c^4$ . The test yields  $\chi^2 = 2543$  for 1106 degrees of freedom. More detailed studies are required in order to understand the precise dynamics of  $\bar{D}^0 \rightarrow K_S\pi^+\pi^-$  decay. However, for the purpose of measuring  $\phi_3$ , we take the fit discrepancy into account in the model uncertainty.

## DALITZ PLOT ANALYSIS OF $B^\pm \rightarrow DK^\pm$ DECAY

The Dalitz plot distributions for the  $\tilde{D} \rightarrow K_S\pi^+\pi^-$  decay are shown in Figs. 5 and 6 for the  $B^\pm \rightarrow \tilde{D}K^\pm$  and  $B^\pm \rightarrow \tilde{D}^*K^\pm$  decays, respectively. These distributions are fitted by minimizing the combined logarithmic likelihood function

$$-2 \log L = -2 \log L_- - 2 \log L_+, \quad (6)$$

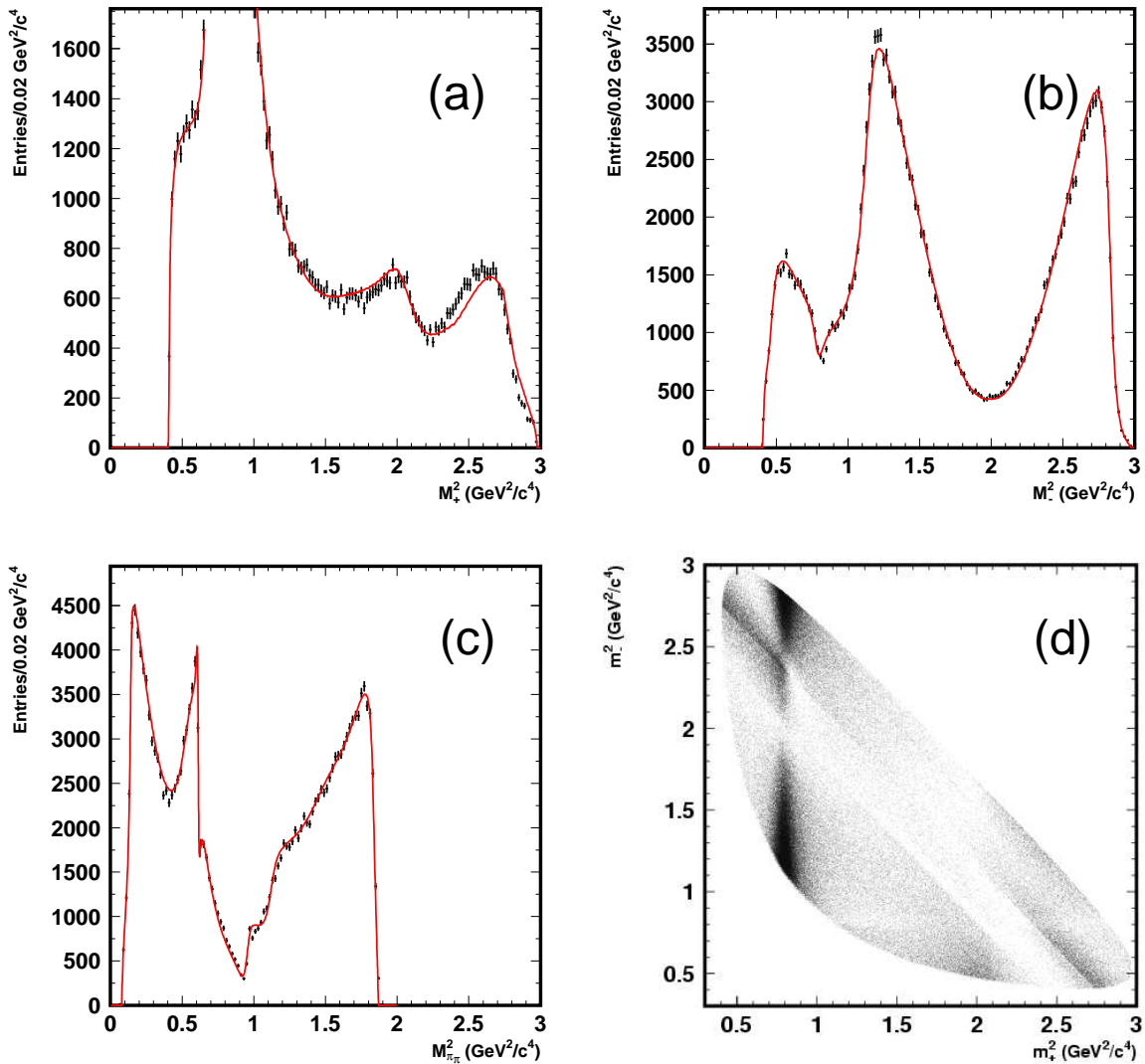


FIG. 4: (a)  $m_+^2$ , (b)  $m_-^2$ , (c)  $m_{\pi\pi}^2$  distributions and (d) Dalitz plot for the  $\bar{D}^0 \rightarrow K_S \pi^+ \pi^-$  decay from the  $D^{*\pm} \rightarrow D \pi_s^\pm$  process. The points with error bars show the data, the smooth curve is the fit result.

where  $L_-(L_+)$  are the likelihoods of  $B^-(B^+)$  data given by Eq. 4. The corresponding Dalitz plot densities  $p_\pm(m_+^2, m_-^2)$  are given by Eq. 5 with decay amplitudes  $M_\pm$  described by Eq. 1 ( $B^+$  data) and Eq. 2 ( $B^-$  data). The  $\bar{D}^0$  decay model  $f$  is fixed, and the free parameters of the fit are the amplitude ratio  $r$  and phases  $\phi_3$  and  $\delta$ .

We consider five sources of background (see Table II), and determine the fraction and Dalitz plot shape for each component. The largest contribution comes from two kinds of continuum events: random combination of tracks, and correctly reconstructed neutral  $D$  mesons combined with random kaons. We estimate their fractions to be  $21.0 \pm 1.7\%$  for  $B^\pm \rightarrow DK^\pm$  and  $9.0 \pm 2.2\%$  for  $B^\pm \rightarrow D^*K^\pm$  using an event sample in which we make



TABLE I: Fit results for  $\bar{D}^0 \rightarrow K_S \pi^+ \pi^-$  decay. Errors are statistical only. The results for the  $\sigma_1$ ,  $\sigma_2$  masses and widths are given in the text.

Intermediate state	Amplitude	Phase ( $^\circ$ )	Fit fraction
$\bar{K}_S \sigma_1$	$1.57 \pm 0.10$	$214 \pm 4$	9.8%
$\bar{K}_S \rho^0$	1.0 (fixed)	0 (fixed)	21.6%
$\bar{K}_S \omega$	$0.0310 \pm 0.0010$	$113.4 \pm 1.9$	0.4%
$\bar{K}_S f_0(980)$	$0.394 \pm 0.006$	$207 \pm 3$	4.9%
$\bar{K}_S \sigma_2$	$0.23 \pm 0.03$	$210 \pm 13$	0.6%
$\bar{K}_S f_2(1270)$	$1.32 \pm 0.04$	$348 \pm 2$	1.5%
$\bar{K}_S f_0(1370)$	$1.25 \pm 0.10$	$69 \pm 8$	1.1%
$\bar{K}_S \rho^0(1450)$	$0.89 \pm 0.07$	$1 \pm 6$	0.4%
$K^*(892)^+ \pi^-$	$1.621 \pm 0.010$	$131.7 \pm 0.5$	61.2%
$K^*(892)^- \pi^+$	$0.154 \pm 0.005$	$317.7 \pm 1.6$	0.55%
$K^*(1410)^+ \pi^-$	$0.22 \pm 0.04$	$120 \pm 14$	0.05%
$K^*(1410)^- \pi^+$	$0.35 \pm 0.04$	$253 \pm 6$	0.14%
$K_0^*(1430)^+ \pi^-$	$2.15 \pm 0.04$	$348.7 \pm 1.1$	7.4%
$K_0^*(1430)^- \pi^+$	$0.52 \pm 0.04$	$89 \pm 4$	0.43%
$K_2^*(1430)^+ \pi^-$	$1.11 \pm 0.03$	$320.5 \pm 1.8$	2.2%
$K_2^*(1430)^- \pi^+$	$0.23 \pm 0.02$	$263 \pm 7$	0.09%
$K^*(1680)^+ \pi^-$	$2.34 \pm 0.26$	$110 \pm 5$	0.36%
$K^*(1680)^- \pi^+$	$1.3 \pm 0.2$	$87 \pm 11$	0.11%
non-resonant	$3.8 \pm 0.3$	$157 \pm 4$	9.7%

TABLE II: Fractions of different background sources.

Background source	$B^\pm \rightarrow DK^\pm$	$B^\pm \rightarrow D^* K^\pm$
$q\bar{q}$ combinatorial	$21.0 \pm 1.7\%$	$9.0 \pm 2.2\%$
$B\bar{B}$ events other than $B^\pm \rightarrow D^{(*)} K^\pm / \pi^\pm$	$2.3 \pm 0.2\%$	$3.1 \pm 0.4\%$
$B^\pm \rightarrow D^{(*)} \pi^\pm$ with $K/\pi$ misID	$0.9 \pm 0.1\%$	$0.7 \pm 0.2\%$
Combinatorics in $D^0$ decay	$0.6 \pm 0.1\%$	$0.6 \pm 0.1\%$
Combinatorial kaon in $B^\pm \rightarrow D^{(*)} K^\pm$ decay	$<0.4\%$ (95% CL)	$<0.4\%$ (95% CL)
Total	$25 \pm 2\%$	$13 \pm 2\%$

requirements that primarily select continuum events but reject  $B\bar{B}$  events. The shape of their Dalitz plot distribution is parameterized by a third-order polynomial in the variables  $m_+^2$  and  $m_-^2$  for the combinatorial background component and a sum of  $D^0$  and  $\bar{D}^0$  shapes for real neutral  $D$  mesons combined with random kaons.

The background from  $B\bar{B}$  events is subdivided into four categories. The  $D^{(*)} K^\pm$  and  $D^{(*)} \pi^\pm$  combinations coming from the decay of  $D^{(*)}$  from one  $B$  meson and  $K^\pm$  and  $\pi^\pm$  from the other  $B$  decay constitute the largest part of the  $B\bar{B}$  background. We obtain their fractions of  $2.3 \pm 0.2\%$  for  $B^\pm \rightarrow DK^\pm$  and  $3.1 \pm 0.4\%$  for  $B^\pm \rightarrow D^* K^\pm$  using a MC study. Their Dalitz plot shapes are parameterized by a second-order polynomial in the variables  $m_+^2$  and  $m_-^2$  for  $B^\pm \rightarrow DK^\pm$  and by a linear function in  $m_+^2$  and  $m_-^2$  plus  $D^0$

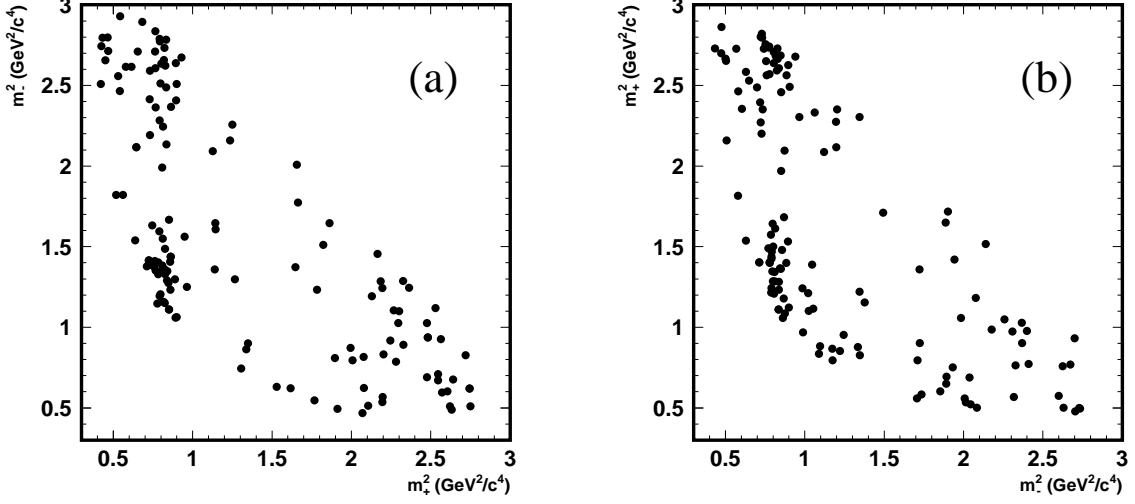


FIG. 5: Dalitz plots of  $\tilde{D} \rightarrow K_S \pi^+ \pi^-$  decay from (a)  $B^+ \rightarrow \tilde{D}K^+$  and (b)  $B^- \rightarrow \tilde{D}K^-$ .

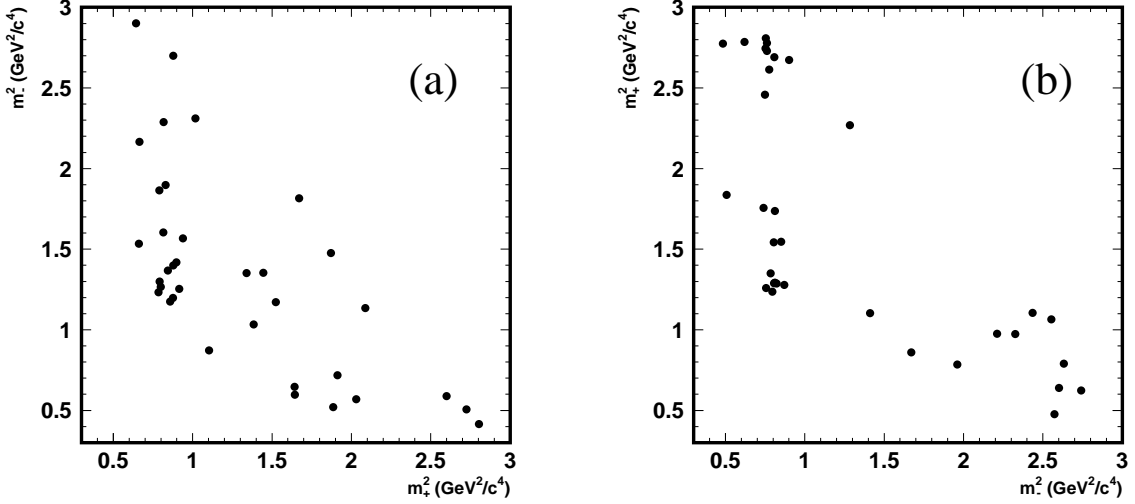


FIG. 6: Dalitz plots of  $\tilde{D} \rightarrow K_S \pi^+ \pi^-$  decay from (a)  $B^+ \rightarrow \tilde{D}^*K^+$  and (b)  $B^- \rightarrow \tilde{D}^*K^-$ .

shape for  $B^\pm \rightarrow D^*K^\pm$ . The background fraction from the process  $B^\pm \rightarrow D^{(*)}\pi^\pm$  with a pion misidentified as a kaon is obtained by fitting the  $\Delta E$  distribution. The corresponding Dalitz plot shape is that of  $\bar{D}^0$  without the opposite flavor admixture. The fractions for this background are  $0.9 \pm 0.1\%$  for  $B^\pm \rightarrow DK^\pm$  and  $0.7 \pm 0.2\%$  for  $B^\pm \rightarrow D^*K^\pm$ . The  $B^\pm \rightarrow D^{(*)}K^\pm$  events where one of the neutral  $D$  meson decay products is combined with a random kaon or pion were studied using a MC data set where one of the charged  $B$  mesons from the  $\Upsilon(4S)$  decays into the  $D^{(*)}K$  state. The estimated background fraction is  $0.6 \pm 0.1\%$  for both  $B^\pm \rightarrow DK^\pm$  and  $B^\pm \rightarrow D^*K^\pm$  modes. The Dalitz plot shape is parameterized by a

linear function in the variables  $m_+^2$  and  $m_-^2$  plus a  $D^0$  amplitude. Events in which a correctly reconstructed neutral  $D$  is combined with a random charged kaon are of importance. A half of the kaons will have the wrong sign and will be misinterpreted as decays of  $D$  mesons of the opposite flavor, thus introducing distortion in the most sensitive area of the Dalitz plot. In the MC sample, we find no events of this kind, which allows us to set an upper limit of 0.4% (at 95% CL) on the fraction for this contribution.

To test the consistency of the fitting procedure, the same fitting procedure is applied to the  $B^\pm \rightarrow \tilde{D}^{(*)}\pi^\pm$  control samples as to the  $B^\pm \rightarrow \tilde{D}^{(*)}K^\pm$  signal. In the case of  $B^\pm \rightarrow \tilde{D}^{(*)}\pi^\pm$ , a small amplitude ratio is expected ( $r \sim |V_{ub}V_{cd}^*|/|V_{cb}V_{ud}^*| \sim 0.01 - 0.02$ ). Here, we consider  $B^+$  and  $B^-$  data separately, to check for the absence of  $CP$  violation. The free parameters of the Dalitz plot fit are  $r_\pm$  and  $\theta_\pm$ , where  $\theta_\pm = \delta \pm \phi_3$ . The fit results for  $B^\pm \rightarrow \tilde{D}\pi^\pm$  sample (3425 events) are  $r_+ = 0.039 \pm 0.021$ ,  $\theta_+ = 240^\circ \pm 28^\circ$  for  $B^+$  data and  $r_- = 0.047 \pm 0.018$ ,  $\theta_- = 193^\circ \pm 24^\circ$  for  $B^-$  data. It should be noted that, since the value of  $r$  is positive definite, the error of this parameter does not serve as a good measure of the  $r \simeq 0$  hypothesis. To demonstrate the deviation of the amplitude ratio  $r$  from zero, the real and imaginary parts of the complex amplitude ratio  $re^{i\theta}$  are more suitable. Figure 7 (a) shows the complex amplitude ratio constraints for the  $B^+$  and  $B^-$  data separately. It can be seen that the amplitude ratios differ from zero by roughly two standard deviations for both cases but are not inconsistent with the expected value of  $r \sim 0.01 - 0.02$ .

The other control sample,  $B^\pm \rightarrow \tilde{D}^*\pi^\pm$  with  $\tilde{D}^*$  decaying to  $\tilde{D}\pi^0$ , also does not show any significant deviation from  $r \simeq 0$ . The results of the fit to the  $B^\pm \rightarrow \tilde{D}^*\pi^\pm$  sample (642 events) are  $r_+ = 0.015 \pm 0.042$ ,  $\theta_+ = 169^\circ \pm 186^\circ$ ,  $r_- = 0.086 \pm 0.049$ ,  $\theta_- = 280^\circ \pm 30^\circ$  and are shown in Fig. 7 (b).

## RESULTS

Fig. 8 shows the constraints on the complex amplitude ratio  $re^{i\theta}$  for the  $B^\pm \rightarrow \tilde{D}K^\pm$  and  $B^\pm \rightarrow \tilde{D}^*K^\pm$  samples. It can be seen that in both signal samples a significant non-zero value of  $r$  is observed. A difference between the phases  $\theta_+$  and  $\theta_-$  is also apparent in both the  $B^\pm \rightarrow \tilde{D}K^\pm$  and  $B^\pm \rightarrow \tilde{D}^*K^\pm$  samples, which indicates a deviation of  $\phi_3$  from zero.

A combined unbinned maximum likelihood fit to the  $B^+$  and  $B^-$  samples with  $r$ ,  $\phi_3$  and  $\delta$  as free parameters yields the following values:  $r = 0.25 \pm 0.07$ ,  $\phi_3 = 64^\circ \pm 15^\circ$ ,  $\delta = 157^\circ \pm 16^\circ$  for the  $B^\pm \rightarrow \tilde{D}K^\pm$  sample and  $r = 0.25 \pm 0.12$ ,  $\phi_3 = 75^\circ \pm 25^\circ$ ,  $\delta = 321^\circ \pm 25^\circ$  for the  $B^\pm \rightarrow \tilde{D}^*K^\pm$  sample. The errors quoted here are obtained from the likelihood fit. These errors are a good representation of the statistical uncertainties for a Gaussian likelihood distribution, however in our case the distributions are highly non-Gaussian. In addition, the errors for the strong and weak phases depend on the values of the amplitude ratio  $r$  (*e.g.* for  $r = 0$  there is no sensitivity to the phases). A more reliable estimate of the statistical uncertainties is obtained using a large number of MC pseudo-experiments as discussed below.

The model used for the  $\bar{D}^0 \rightarrow K_S\pi^+\pi^-$  decay is one of the main sources of systematic error for our analysis. Since the Dalitz density is proportional to the absolute value squared of the decay amplitude, the phase  $\phi(m_+^2, m_-^2)$  of the complex amplitude is not directly measured. The phase variations across the Dalitz plot distribution are therefore the result of model assumptions.

A MC simulation is used for estimating the effects of the model uncertainties. Event samples are generated according to the Dalitz plot distribution described by the amplitude given by Eq. 1 with the resonance parameters extracted from our fit of continuum  $D^0$  data.

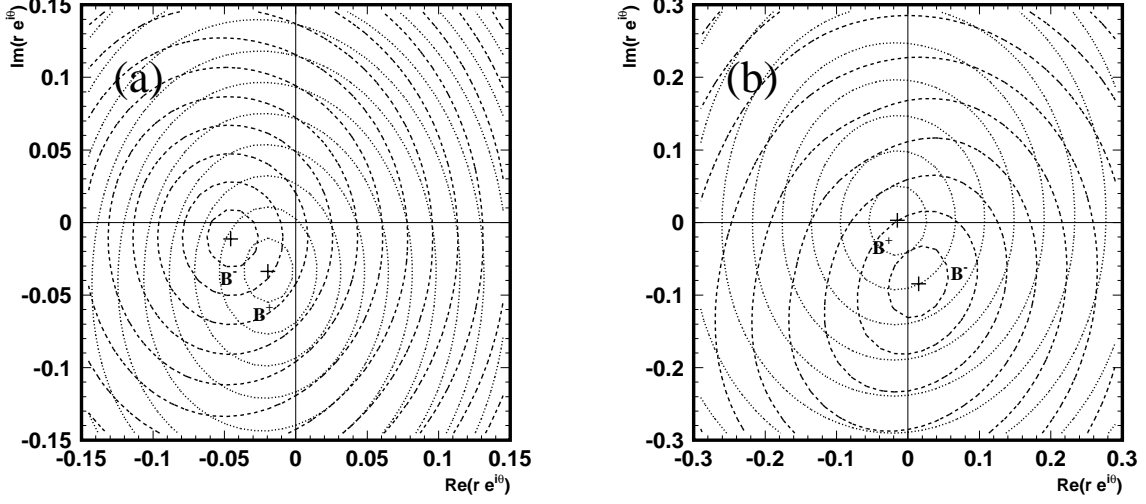


FIG. 7: Constraint plots of the complex amplitude ratio  $re^{i\theta}$  for (a)  $B^\pm \rightarrow \tilde{D}\pi^\pm$  and (b)  $B^\pm \rightarrow \tilde{D}^*\pi^\pm$  decays. Contours indicate integer multiples of the standard deviation. Dotted contours are from  $B^+$  data, dashed contours are from  $B^-$  data.

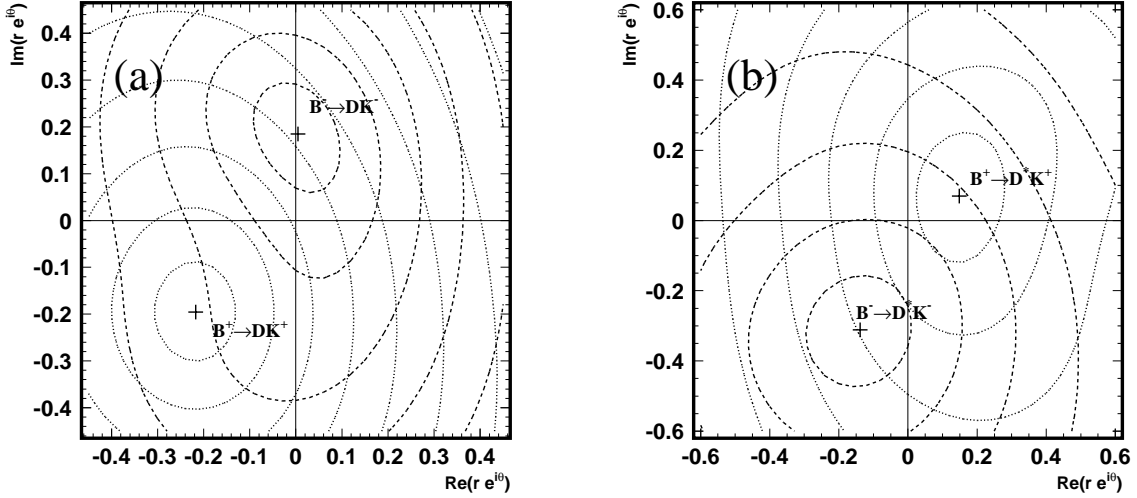


FIG. 8: Constraint plots of the complex amplitude ratio  $re^{i\theta}$  for (a)  $B^\pm \rightarrow \tilde{D}K^\pm$  and (b)  $B^\pm \rightarrow \tilde{D}^*K^\pm$  decays. Contours indicate integer multiples of the standard deviation. Dotted contours are from  $B^+$  data, dashed contours are from  $B^-$  data.

We then fit the distribution using different models for  $f(m_+, m_-)$  (see Table III). We scan the phases  $\phi_3$  and  $\delta$  in their physical regions and take the maximum deviations of the fit parameters ( $(\Delta r)_{\max}$ ,  $(\Delta\phi_3)_{\max}$ , and  $(\Delta\delta)_{\max}$ ) as model uncertainty estimates. The values for  $(\Delta r)_{\max}$ ,  $(\Delta\phi_3)_{\max}$  and  $(\Delta\delta)_{\max}$  quoted in Table III are obtained with the value  $r = 0.13$ .

TABLE III: Estimation of model uncertainty.

Fit model	$(\Delta r)_{\max}$	$(\Delta\phi_3)_{\max}$ ( $^\circ$ )	$(\Delta\delta)_{\max}$ ( $^\circ$ )
$F_r = F_D = 1$	0.01	3.1	3.3
$\Gamma(q^2) = \text{Const}$	0.02	4.7	9.0
Narrow resonances plus non-resonant term	0.03	9.9	18.2
Total	0.04	11	21

For larger  $r$  values, the model uncertainty tends to be smaller, so our estimate of the model uncertainty is conservative.

All the fit models are based on Breit-Wigner parameterizations of resonances. Since a Breit-Wigner amplitude can only describe narrow resonances well, the usual technique to deal with broad states is to introduce Blatt-Weisskopf form factors for the  $\bar{D}^0$  meson ( $F_D$ ) and intermediate resonance ( $F_r$ ) and a  $q^2$ -dependence of the resonance width  $\Gamma$ . These quantities have substantial theoretical uncertainties. We therefore use a fit without Blatt-Weisskopf form factors and with a constant resonance width to estimate such an error. We also use a model containing only narrow resonances ( $K^*(892)$ ,  $\rho$ , doubly Cabibbo-suppressed  $K^*(892)$  and  $f^0(980)$ ) with the wide ones approximated by the flat non-resonant term. The study of the model errors is summarized in Table III. Our estimate of the systematic uncertainty on  $\phi_3$  is  $11^\circ$ .

There are other potential sources of systematic error such as uncertainties in the background Dalitz density, efficiency variations over the phase space,  $m_{\pi\pi}^2$  resolution, and possible fit biases. These are listed in Table IV for the  $B^\pm \rightarrow \bar{D}K^\pm$  and  $B^\pm \rightarrow \bar{D}^*K^\pm$  modes separately. The effect of background Dalitz density is estimated by extracting the background shape parameters from the  $M_D$  sidebands and by using a flat background distribution. The maximum deviation of the fit parameters from the “standard” background parameterization is assigned as the corresponding systematic error. The effect of the uncertainty in the background fraction is studied by varying the background fraction by one standard deviation. The efficiency shape and  $m_{\pi\pi}^2$  resolution are extracted from the MC simulations. To estimate their contributions to the systematic error, we repeat the fit using a flat efficiency and a fit model that does not take the resolution into account, respectively. The biases due to the efficiency shape differ for  $B^\pm \rightarrow \bar{D}K^\pm$  and  $B^\pm \rightarrow \bar{D}^*K^\pm$  samples, but since we expect the values of the efficiency systematics to be close for the two modes, we assign the maximum value of the bias as the corresponding systematic error.

We use a frequentist technique to evaluate the statistical significance of the measurements. To obtain the probability density function (PDF) of the fitted parameters as a function of the true parameters, which is needed for this method, we employ a “toy” MC technique that uses a simplified MC simulation of the experiment which incorporates the same efficiencies, resolution and backgrounds as used in the data fit. This MC is used to generate several hundred experiments for a given set of  $r$ ,  $\theta_+$  and  $\theta_-$  values. For each simulated experiment, Dalitz plot distributions are generated with equal numbers of events as in the data, 137 and 139 events for  $B^-$  and  $B^+$  decays, correspondingly, for  $B^\pm \rightarrow \bar{D}K^\pm$  mode and 34 and 35 events for  $B^-$  and  $B^+$  for  $B^\pm \rightarrow \bar{D}^*K^\pm$  mode. The simulated Dalitz plot distributions are subjected to the same fitting procedure that is applied to the data. This is repeated for different values of  $r$ , producing distributions of the fitted parameters that are used to

TABLE IV: Contributions to the experimental systematic error.

Source	$B^\pm \rightarrow \tilde{D}K^\pm$			$B^\pm \rightarrow \tilde{D}^*K^\pm$		
	$\Delta r$	$\Delta\phi_3$ (°)	$\Delta\delta$ (°)	$\Delta r$	$\Delta\phi_3$ (°)	$\Delta\delta$ (°)
Background shape	0.027	5.7	4.1	0.014	3.1	5.3
Background fraction	0.006	0.2	1.0	0.005	0.7	1.4
Efficiency shape	0.012	4.9	2.4	0.002	3.5	1.0
$m_{\pi\pi}^2$ resolution	0.002	0.3	0.3	0.002	1.7	1.4
Control sample bias	0.004	10.2	10.2	0.004	9.9	9.9
Total	0.03	13	11	0.02	11	11

produce a functional form of the PDFs of the reconstructed values for any set of input parameters.

We parameterize the PDF of a set of fit parameters  $(r, \phi_3, \delta)$ , assuming the errors of parameters  $\text{Re}(r_\pm e^{i\theta_\pm})$  and  $\text{Im}(r_\pm e^{i\theta_\pm})$  are uncorrelated and have Gaussian distributions with equal RMS which we denote as  $\sigma$ . The PDF of the parameters  $(r_\pm, \theta_\pm)$  for the true parameters  $(\bar{r}_\pm, \bar{\theta}_\pm)$  is thus written as

$$d^2P(r_\pm, \theta_\pm | \bar{r}_\pm, \bar{\theta}_\pm) = \frac{1}{2\pi\sigma^2} \exp \left[ -\frac{(r_\pm \cos \theta_\pm - \bar{r} \cos \bar{\theta}_\pm)^2 + (r_\pm \sin \theta_\pm - \bar{r} \sin \bar{\theta}_\pm)^2}{2\sigma^2} \right] r_\pm dr_\pm d\theta_\pm. \quad (7)$$

To obtain the PDF for the parameters  $(r, \phi_3, \delta)$  we fix  $r = r_+ = r_-$  and substitute the total phases with  $\delta + \phi_3$  and  $\delta - \phi_3$ :

$$\frac{d^3P}{drd\phi_3d\delta}(r, \phi_3, \delta | \bar{r}, \bar{\phi}_3, \bar{\delta}) = \frac{d^2P}{dr_+d\theta_+}(r, \delta + \phi_3 | \bar{r}, \bar{\delta} + \bar{\phi}_3) \frac{d^2P}{dr_-d\theta_-}(r, \delta - \phi_3 | \bar{r}, \bar{\delta} - \bar{\phi}_3). \quad (8)$$

There is only one free parameter  $\sigma$  which is obtained from the unbinned maximum likelihood fit of the MC distribution to Eq. 8. The value of  $\sigma$  is equal to 0.10 for the  $B^\pm \rightarrow \tilde{D}K^\pm$  decay and  $\sigma = 0.18$  for the  $B^\pm \rightarrow \tilde{D}^*K^\pm$  decay.

Once the PDF is obtained, we can calculate the confidence level  $\alpha$  for each set of true parameters  $(\bar{r}, \bar{\phi}_3, \bar{\delta})$  for given measurements,  $(r, \phi_3, \delta) = (0.25, 64^\circ, 157^\circ)$  for the  $\tilde{D}K^\pm$  mode and  $(0.25, 75^\circ, 321^\circ)$  for the  $\tilde{D}^*K^\pm$  mode. The confidence regions for the pairs of parameters  $(\phi_3, \delta)$  and  $(\phi_3, r)$  are shown in Fig. 9 ( $B^\pm \rightarrow \tilde{D}K^\pm$  mode) and Fig. 10 ( $B^\pm \rightarrow \tilde{D}^*K^\pm$  mode). They are the projections of the corresponding confidence regions in the three-dimensional parameter space. We show the 20%, 74% and 97% confidence level regions, which correspond to one, two, and three standard deviations for a three-dimensional Gaussian distribution.

For the final results, we use the central values that are obtained by maximizing the PDF and the statistical errors corresponding to the 20% confidence region (one standard deviation). Of the two possible solutions  $(\phi_3, \delta)$  and  $(\phi_3 + 180^\circ, \delta + 180^\circ)$  we choose the one with  $0 < \phi_3 < 180^\circ$ . The final results are

$$r = 0.21 \pm 0.08 \pm 0.03 \pm 0.04, \quad \phi_3 = 64^\circ \pm 19^\circ \pm 13^\circ \pm 11^\circ, \quad \delta = 157^\circ \pm 19^\circ \pm 11^\circ \pm 21^\circ \quad (9)$$

for the  $B^\pm \rightarrow \tilde{D}K^\pm$  mode and

$$r = 0.12_{-0.11}^{+0.16} \pm 0.02 \pm 0.04, \quad \phi_3 = 75^\circ \pm 57^\circ \pm 11^\circ \pm 11^\circ, \quad \delta = 321^\circ \pm 57^\circ \pm 11^\circ \pm 21^\circ \quad (10)$$



for the  $B^\pm \rightarrow \tilde{D}^* K^\pm$  mode. The first, second, and third errors are statistical, systematic, and model dependent errors.

While the  $\phi_3$  and  $\delta$  values that are determined from the toy MC are consistent with those that are determined in the unbinned maximum likelihood fits for both  $\tilde{D}K^\pm$  and  $\tilde{D}^*K^\pm$ , the corresponding  $r$  values are significantly different. This is due to a bias in the unbinned maximum likelihood. Since  $r$  is a positive-definite quantity, the fit tends to return a larger value for  $r$  than its true value, particularly when  $r$  is small.

In the frequentist approach, the significance of  $CP$  violation is evaluated by finding the confidence level for the most probable  $CP$  conserving point, *i.e.* the point with  $r = 0$  or  $\phi_3 = 0$ , for which the confidence level  $\alpha(\bar{r}, \bar{\phi}_3, \bar{\delta})$  is minimal. This procedure gives  $\alpha = 94\%$  for the  $B^\pm \rightarrow \tilde{D}K^\pm$  sample and  $\alpha = 38\%$  for  $B^\pm \rightarrow \tilde{D}^*K^\pm$ .

The two events samples,  $B^\pm \rightarrow DK^\pm$  and  $B^\pm \rightarrow D^*K^\pm$ , are combined in order to obtain a more accurate measurement of  $\phi_3$ . The technique we use to obtain the combined measurement is also based on a frequentist approach. Here we have five true parameters ( $\bar{\phi}_3, \bar{r}_1, \bar{r}_2, \bar{\delta}_1$  and  $\bar{\delta}_2$ , where the indices 1 and 2 correspond to  $B^\pm \rightarrow DK^\pm$  and  $B^\pm \rightarrow D^*K^\pm$  modes, respectively) and six reconstructed parameters ( $r, \phi_3$  and  $\delta$  for each of the two modes). The PDF for the reconstructed parameters is written as

$$\frac{dP}{dx}(x, \mu) = \frac{d^3 P_{B \rightarrow D^0 K}}{dr d\phi_3 d\delta}(r_1, (\phi_3)_1, \delta_1 | \bar{r}_1, \bar{\phi}_3, \bar{\delta}_1) \frac{d^3 P_{B \rightarrow D^* K}}{dr d\phi_3 d\delta}(r_2, (\phi_3)_2, \delta_2 | \bar{r}_2, \bar{\phi}_3, \bar{\delta}_2), \quad (11)$$

where  $x = (dr_1, d(\phi_3)_1, d\delta_1, dr_2, d(\phi_3)_2, d\delta_2)$  is a vector of the reconstructed parameters, and  $\mu = (\bar{\phi}_3, \bar{r}_1, \bar{r}_2, \bar{\delta}_1, \bar{\delta}_2)$  is a vector of the true parameters. Using this PDF and Feldman-Cousins likelihood ratio ordering [14], we can calculate the confidence level  $\alpha(\mu)$ . This approach gives  $\phi_3 = 68^\circ$  as the central value. The one standard deviation interval for  $\phi_3$  (which corresponds to the 3.7% confidence level for the case of a five-dimensional Gaussian distribution) is  $\phi_3 = 68^\circ \begin{smallmatrix} +14^\circ \\ -15^\circ \end{smallmatrix}$ .

Since the  $B^\pm \rightarrow DK^\pm$  contribution dominates in the combined measurement, we use its value of the systematic uncertainty, which is  $13^\circ$ , as an estimate of the systematic uncertainty in the combined  $\phi_3$  measurement. The  $\phi_3$  result from the combined analysis is

$$\phi_3 = 68^\circ \begin{smallmatrix} +14^\circ \\ -15^\circ \end{smallmatrix} \pm 13^\circ \pm 11^\circ, \quad (12)$$

where the first error is statistical, the second is experimental systematics, and the third is model uncertainty. The two standard deviation interval including the systematic and model uncertainties is  $22^\circ < \phi_3 < 113^\circ$ . The statistical significance of  $CP$  violation for the combined measurement is 98%.

## CONCLUSION

We report results of a measurement of the unitarity triangle angle  $\phi_3$  that uses a method based on a Dalitz plot analysis of the three-body  $D$  decay in the process  $B^\pm \rightarrow D^{(*)}K^\pm$ . The measurement of  $\phi_3$  using this technique was performed based on  $253 \text{ fb}^{-1}$  data sample collected by the Belle detector. From the combination of  $B^\pm \rightarrow DK^\pm$  and  $B^\pm \rightarrow D^*K^\pm$  modes, we obtain the value of  $\phi_3 = 68^\circ \begin{smallmatrix} +14^\circ \\ -15^\circ \end{smallmatrix} \pm 13^\circ \pm 11^\circ$  (solution with  $0 < \phi_3 < 180^\circ$ ). The first error is statistical, the second is experimental systematics and the third is model uncertainty. The two standard deviation interval (including model and systematic uncertainties) is  $22^\circ < \phi_3 < 113^\circ$ . The statistical significance of  $CP$  violation for the combined

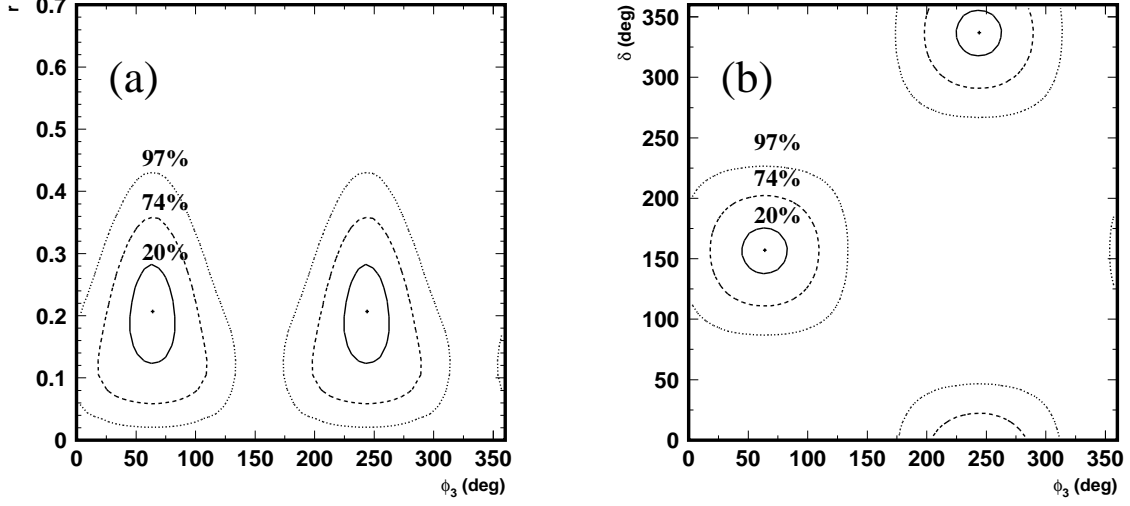


FIG. 9: Confidence regions for the pairs of parameters (a)  $(r, \phi_3)$  and (b)  $(\phi_3, \delta)$  for the  $B^\pm \rightarrow \tilde{D}K^\pm$  sample.

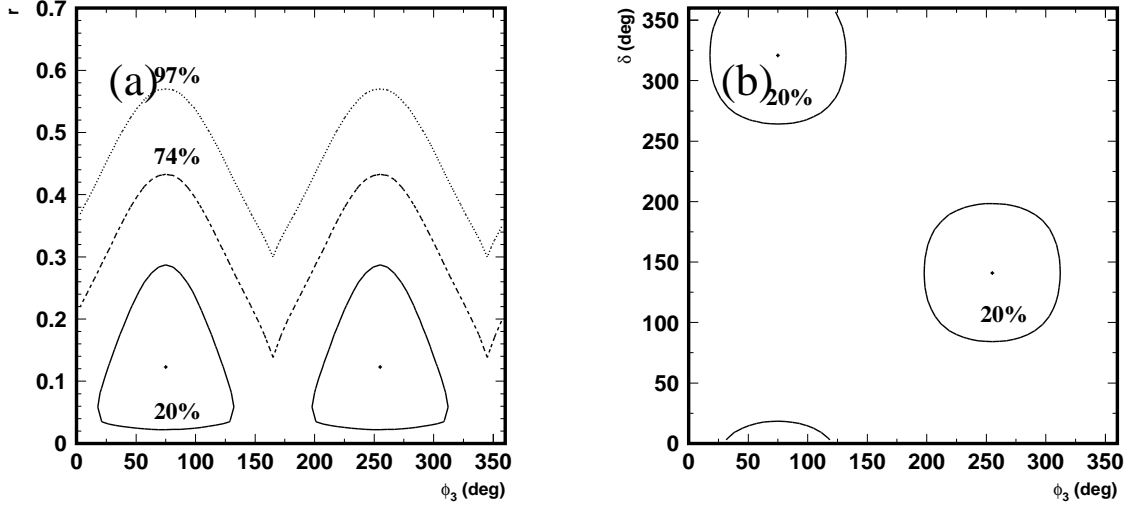


FIG. 10: Confidence regions for the pairs of parameters (a)  $(r, \phi_3)$  and (b)  $(\phi_3, \delta)$  for the  $B^\pm \rightarrow \tilde{D}^*K^\pm$  sample.

measurement is 98%. The method allows us to obtain a value of the amplitude ratio  $r$ , which can be used in other  $\phi_3$  measurements. We obtain  $r = 0.21 \pm 0.08 \pm 0.03 \pm 0.04$  for the  $B^\pm \rightarrow DK^\pm$  mode and  $r = 0.12^{+0.16}_{-0.11} \pm 0.02 \pm 0.04$  for the  $B^\pm \rightarrow D^*K^\pm$  mode.

## Acknowledgments

We are grateful to V. Chernyak and M. Gronau for fruitful discussions. We thank the KEKB group for the excellent operation of the accelerator, the KEK Cryogenics group for the efficient operation of the solenoid, and the KEK computer group and the National Institute of Informatics for valuable computing and Super-SINET network support. We acknowledge support from the Ministry of Education, Culture, Sports, Science, and Technology of Japan and the Japan Society for the Promotion of Science; the Australian Research Council and the Australian Department of Education, Science and Training; the National Science Foundation of China under contract No. 10175071; the Department of Science and Technology of India; the BK21 program of the Ministry of Education of Korea and the CHEP SRC program of the Korea Science and Engineering Foundation; the Polish State Committee for Scientific Research under contract No. 2P03B 01324; the Ministry of Science and Technology of the Russian Federation; the Ministry of Education, Science and Sport of the Republic of Slovenia; the National Science Council and the Ministry of Education of Taiwan; and the U.S. Department of Energy.

---

\* on leave from Nova Gorica Polytechnic, Nova Gorica

- [1] M. Kobayashi and T. Maskawa, Prog. Theor. Phys. **49**, 652 (1973); N. Cabibbo, Phys. Rev. Lett. **10**, 531 (1963);
- [2] M. Gronau and D. London, Phys. Lett. **B253**, 483 (1991); M. Gronau and D. Wyler, Phys. Lett. **B265**, 172 (1991).
- [3] I. Dunietz, Phys. Lett. **B270**, 75 (1991).
- [4] D. Atwood, G. Eilam, M. Gronau and A. Soni, Phys. Lett. **B341**, 372 (1995).
- [5] D. Atwood, I. Dunietz and A. Soni, Phys. Rev. Lett. **78**, 3257 (1997); D. Atwood, I. Dunietz and A. Soni, Phys. Rev. D **63**, 036005 (2001).
- [6] A. Giri, Yu. Grossman, A. Soffer, J. Zupan, Phys. Rev. D **68**, 054018 (2003).  
This technique was proposed independently in the Belle Collaboration, and the analysis of experimental data was under way before the A. Giri *et al.* publication appeared (Proceedings of BINP Special Analysis Meeting on Dalitz Analysis, 24-26 Sep. 2002, unpublished).
- [7] Belle Collaboration, A. Poluektov *et al.*, Phys. Rev. D **70**, 072003 (2004).
- [8] BABAR Collaboration, B. Aubert *et al.*, hep-ex/0408088.
- [9] Belle Collaboration, A. Abashian *et al.*, Nucl. Instr. and Meth. A **479**, 117 (2002).
- [10] CLEO Collaboration, H. Muramatsu *et al.*, Phys. Rev. Lett. **89**, 251802 (2002), Erratum-ibid: **90**, 059901 (2003).
- [11] CLEO Collaboration, S. Kopp *et al.*, Phys. Rev. D **63**, 092001 (2001).
- [12] G.J. Gounaris, J.J. Sakurai, Phys. Rev. Lett. **21**, 24 (1968).
- [13] E791 Collaboration, E. M. Aitala *et al.*, Phys. Rev. Lett. **86**, 765 (2001).
- [14] G. J. Feldman and R. D. Cousins, Phys. Rev. D **57**, 3873 (1998).